HHS Public Access

Author manuscript

ACS Appl Mater Interfaces. Author manuscript; available in PMC 2019 July 12.

Published in final edited form as:

ACS Appl Mater Interfaces. 2016 December 21; 8(50): 34194–34197. doi:10.1021/acsami.6b14468.

Micropatterned Polymer Nanorod Forests and Their Use for Dual Drug Loading and Regulation of Cell Adhesion

Chunlei Zhu[†], **Jiajia Xue**[†], **Kyle D. Gilroy**[†], **Da Huo**[†], **Song Shen**[†], and **Younan Xia**[*,†,‡]

[†]The Wallace H. Coulter Department of Biomedical Engineering, Georgia Institute of Technology and Emory University, Atlanta, Georgia 30332, United States

[‡]School of Chemistry and Biochemistry, School of Chemical and Biomolecular Engineering, Georgia Institute of Technology, Atlanta, Georgia 30332, United States

Abstract

This paper describes a simple method for the fabrication of micropatterned polymer nanorod forests by templating against the channels in an anodized aluminum oxide membrane partially masked by gelatin. The nanorod forests easily support bimodal drug loading, with one drug encapsulated in the nanorods and the other physisorbed on their surface. During cell culture, preosteoblasts are predominantly attracted to the nanorod forests and driven to climb up along the nanorods. This type of scaffold integrates both microscale and nanoscale features into a single substrate, holding great potential for applications in cell culture and tissue engineering.

Graphical abstract

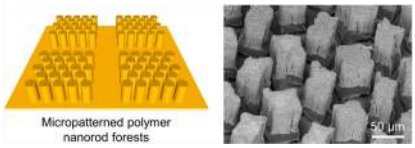

Keywords

micropatterning nanorod forests; dual drug loading; cell adhesion; tissue engineering

Nanostructured surfaces and/or materials offer a unique platform to investigate cell-environment interactions by providing a customized microenvironment that contains both physical and chemical cues.[1–6] Polymer nanorods are particularly well-suited for such studies because of their enhanced biocompatibility and drug loading capability when compared to their inorganic counterparts.[7–10] Recently, substrates patterned with arrays of

[*]**Corresponding Author**: younan.xia@bme.gatech.edu.

Supporting Information

The Supporting Information is available free of charge on the ACS Publications website at DOI: 10.1021/acsami.6b14468. Experimental methods, SEM images of an AAO membrane, a tilted SEM image of the gelatin-masked AAO membrane, MFIs of RhB and FITC-BSA at the base film and top surface of the nanorod forests, drug release profiles, and a 3D profile showing the distribution of MC3T3-E1 cells along the micropatterned nanorod forests (PDF)

The authors declare no competing financial interest.

polymer nanorods have been demonstrated to facilitate rapid drug localization and topographical cellular control.[11] However, the fabrication was based upon photolithography, which is expensive and less accessible to chemists, biochemists, and biologists.[12] In addition, the resulting polymer nanorods are prone to collapse as a result of the insufficient extrusion of polymers into the template, impairing their capability to effectively regulate cell behavior.

Herein, we report a simple, rapid, and cost-effective method for fabricating micropatterned arrays of polymer nanorods (Scheme 1). In a typical process, electrospray was employed to deposit a thin layer of gelatin on a nylon mesh with microscale openings. The micropatterned gelatin network was then transferred onto an anodized aluminum oxide (AAO) membrane (Figure S1), which is widely used as a template for the fabrication of nanorod and nanotube arrays.[11,13,14] After infiltrating the unblocked channels with a poly(lactic-co-glycolic acid) (PLGA) solution, both the AAO template and gelatin network were selectively removed, leaving behind a polymer substrate patterned with an array of nanorod forests. The interiors of the nanorods, the gaps among the nanorods, and the open space between adjacent nanorod forests, could all be used for the drug loading and/or cell seeding.

Figure 1a shows the optical and electron micrographs of a woven nylon mesh. The mesh opening and spacing were 41 and 25 μm, respectively, which provide enough space for the nanorod forests to stand up and, at the same time, for the cells to reside and remodel. Electrospray was used to coat the nylon mesh with a thin layer of gelatin. Under a strong electric field, the liquid jet was directed toward the nylon mesh. Over time, the mesh openings decreased as a result of the accumulation of gelatin on the nylon backbone (Figure 1b). The gelatin layer deposited on the nylon mesh was then transferred onto the surface of an AAO membrane with the assistance of aqueous ethanol solution. The dissolved gelatin could flow along the nylon backbone and enter the space between the nylon mesh and the AAO membrane. After drying, the nylon mesh was carefully peeled off, leaving behind a meshed network of gelatin on the surface of the AAO membrane (Figure 1c). The transfer-printed gelatin had a concave, canoe-like morphology (Figure S2), primarily due to the woven structure of the nylon mesh. As shown in Figure 1d, the channels in the AAO membrane were completely blocked in the regions covered by gelatin, effectively preventing the channels from being infiltrated by PLGA.

Although it is straightforward to fill the channels by directly adding PLGA solution onto the surface-patterned AAO membrane, this process can be easily compromised if the excess fluid also enters the channels from the opposite side of the membrane. To avoid this problem, a smear-dip-push strategy was adopted. Specifically, 2.5 μL of PLGA solution was added onto a glass slide and smeared with a blunt pipet tip to form a thin liquid film. The surface-patterned AAO membrane was then carefully placed on top of the liquid film and laterally moved with tweezers to evenly wet the surface. In principle, this simple method works well for all hydrophobic polymers that can be dissolved in 1,4-dioxane to obtain polymer solutions with reasonable viscosity for easy trapping in the channels. After drying under ambient conditions, the procedure was repeated one more time to make the resultant scaffold more robust. Finally, the AAO template was selectively dissolved by etching with

10% phosphoric acid. As anticipated, the resultant scaffold contained an array of PLGA nanorod forests over an area of 4 mm × 4 mm. Each forest was approximately 30–40 μm in lateral width and 60–70 μm in height. These dimensions reflect the confinement by the AAO template and the patterned gelatin mask. As shown in Figure 2a, b, each forest had well defined edges, with the densely packed nanorods bound together to the underlying base film. Compared with the original pore size of the nylon mesh, the nanorod forests exhibited slightly reduced lateral dimensions due to the spreading of gelatin from the nylon backbone (Figure 1c and Figure S2). The oblique-view images shown in Figure 2c, d demonstrate that the resultant PLGA nanorods possessed essentially the same alignment as determined by the channels in the AAO template. From the images in Figure 2d and Figure S2, the overall height of the resultant scaffold was 70–90 μm, with the nanorod forests accounting for 60–70 μm and the base film contributing the other 10–20 μm.

We next used two fluorescent agents as the model compounds to demonstrate dual drug loading. Specifically, Rhodamine B (RhB) was dissolved in the PLGA solution and then infiltrated into the channels of the gelatin-masked AAO membrane. After template removal, the scaffold was wetted with aqueous albumin-fluorescein isothiocyanate conjugate (FITC-BSA) solution and dried using filter paper. The distributions of the loaded compounds were examined using confocal laser scanning microscopy (CLSM). As shown in Figure 3a, b, both RhB and FITC-BSA were easily identified at the top surface of each nanorod forest, and the fluorescent patterns were essentially the same as the outlines of the nanorod forests. Despite some colocalization, the fluorescence signals from RhB and FITC-BSA did not fully overlap due to their different loading methods (Figure 3c). We also measured their distributions at the base film, where nearly no signal from FITC-BSA was detected. In contrast, RhB was evenly distributed due to its encapsulation in the PLGA substrate (Figure 3d). It should be pointed out that the fluorescence intensity from the interior of each nanorod forest was much weaker than that from the exterior, which can be attributed to the inefficient transmission of the emitted light through the densely packed nanorods. The three-dimensional (3D) profile reconstructed from Z-stack images shows that the physisorbed FITC-BSA was predominantly enriched at the top of each nanorod forest and superimposed with the broadly distributed RhB (Figure 3e). The mean fluorescence intensities (MFIs) of RhB and FITC-BSA at the top surface of nanorod forests were 3.7 and 118 times as great as those at the base film, respectively (Figure S3). The cross-sectional image shown in Figure 3f further demonstrates the graded distribution of FITC-BSA along the nanorod forests with the maximum adsorption near the top, which is probably caused by the capillary action between nanorods during filter paper wiping. We also tested the release profiles of RhB and FITC-BSA from the drug loaded nanorod forests. The result shown in Figure S4 demonstrates that FITC-BSA exhibited a fast and complete release within 48 h, while RhB showed a slow and sustained release under the same conditions. A multidrug release system is highly desired when two or more biofactors need to be released with well-defined and controllable profiles, such as in wound healing.[15]

To investigate the effectiveness of cell adhesion to the micropatterned nanorod forests, we cultured mouse-derived preosteoblasts (MC3T3-E1), the most commonly used cell line for the study of cell responses to structured surfaces, on the engineered scaffold.[16–18] To make a comparison, we also seeded cells onto a glass coverslip and a nonpatterned array of

nanorods. After incubation for 24 h, the cells were stained with calcein AM to visualize the cytoplasm. Figure 4a–c show the superimposed confocal images of preosteoblasts cultured on these substrates. On the nonpatterned surfaces, the cells exhibited random adhesion and spreading. In contrast, the cells primarily adhered to the side surfaces of the nanorod forests, exhibiting a quasi-square fluorescent pattern. It should be noted that the preosteoblasts were rarely seen on the base film, which can be ascribed to their enhanced adhesion toward the rough surfaces presented by the nanorods.[16,17] To determine the spatial distribution of the preosteoblasts on the nanorod forests, a series of Z-stack images were collected. The 3D reconstruction image reveals that the majority of the cells were localized in a region 20–60 μm away from the base film (Figure S5). We also conducted SEM characterization to gain more insight into the interactions between the preosteoblasts and the substrates (Figure 4d–f). On the nonpatterned substrates, the cells were randomly distributed and highly flattened, suggesting their strong interactions with the underlying surfaces. Interestingly, the cells adhered strongly to the nanorod forests from all exposed directions, with some preosteoblasts occupying the top surface of each forest or stretching across the forests, indicating a concerted effect of the hierarchical structures on cell adhesion.

In summary, we have developed a simple and versatile method for fabricating micropatterned polymer nanorod forests. The fabrication process is electrospray-assisted and all experimental components are commercially available, making such a method simple and cost-effective. Moreover, the created architecture can be easily modulated by varying the fabrication parameters, such as electrospray time, the dimensions of the nylon mesh, and the features of the AAO membrane (e.g., channel-diameter and interchannel spacing). The hierarchical structure can be used for dual drug loading and regulation of cell adhesion, holding great potential for a number of applications. For example, in the process of wound healing, one drug, such as a growth factor, can be physisorbed on the surface of the nanorods to promote rapid cell adhesion and proliferation. Meanwhile, another drug, such as an antibiotic, can be encapsulated in the nanorods for sustained release to prevent wound infection. Over time, the scaffold will degrade and eventually integrate with the host tissue. Furthermore, such a hierarchical scaffold can be used to recapitulate stem-cell niches by loading specific adhesion molecules, growth factors, extracellular matrices, and/or a layer of feeder cells. As a result, one can create 3D in vitro microenvironment for stem cells to interact with, providing valuable information to understand the self-renewal and differentiation of stem cells.

Supplementary Material

Refer to Web version on PubMed Central for supplementary material.

ACKNOWLEDGMENTS

This work was supported in part by a grant from the National Institutes of Health (R01 AR060820) and startup funds from the Georgia Institute of Technology.

REFERENCES

(1). Mendes PM Cellular Nanotechnology: Making Biological Interfaces Smarter. Chem. Soc. Rev 2013, 42, 9207–9218. [PubMed: 24097313]

(2). Kerativitayanan P; Carrow JK; Gaharwar AK Nanomaterials for Engineering Stem Cell Responses. Adv. Healthcare Mater 2015, 4, 1600–1627.

(3). Bettinger CJ; Langer R; Borenstein JT Engineering Substrate Topography at the Micro and Nanoscale to Control Cell Function. Angew. Chem., Int. Ed 2009, 48, 5406–5415.

(4). Dalby MJ; Gadegaard N; Oreffo RO Harnessing Nanotopography and Integrin-Matrix Interactions to Influence Stem Cell Fate. Nat. Mater 2014, 13, 558–569. [PubMed: 24845995]

(5). Mpoyi EN; Cantini M; Reynolds PM; Gadegaard N; Dalby MJ; Salmerón-Sânchez M Protein Adsorption as a Key Mediator in the Nanotopographical Control of Cell Behavior. ACS Nano 2016, 10, 6638–6647. [PubMed: 27391047]

(6). Kwak M; Han L; Chen JJ; Fan R Interfacing Inorganic Nanowire Arrays and Living Cells for Cellular Function Analysis. Small 2015, 11, 5600–5610. [PubMed: 26349637]

(7). Porter JR; Henson A; Popat KC Biodegradable Poly(ε-caprolactone) Nanowires for Bone Tissue Engineering Applications. Biomaterials 2009, 30, 780–788. [PubMed: 19012962]

(8). Leszczak V; Baskett DA; Popat KC Smooth Muscle Cell Functionality on Collagen Immobilized Polycaprolactone Nanowire Surfaces. J. Fund. Biomater 2014, 5, 58–77.

(9). Leszczak V; Baskett DA; Popat KC Endothelial Cell Growth and Differentiation on Collagen-Immobilized Polycaprolactone Nanowire Surfaces. J. Biomed. Nanotechnol 2015, 11, 1080–1092. [PubMed: 26353596]

(10). Jiang S; Sun Y; Cui X; Huang X; He Y; Ji S; Shi W; Ge D Enhanced Drug Loading Capacity of Polypyrrole Nanowire Network for Controlled Drug Release. Synth. Met 2013, 163, 19–23.

(11). Fox CB; Kim J; Schlesinger EB; Chirra HD; Desai TA Fabrication of Micropatterned Polymeric Nanowire Arrays for High Resolution Reagent Localization and Topographical Cellular Control. Nano Lett. 2015, 15, 1540–1546. [PubMed: 25639724]

(12). Qin D; Xia Y; Whitesides GM Soft Lithography for Micro and Nanoscale Patterning. Nat. Protoc 2010, 5, 491–502. [PubMed: 20203666]

(13). Martin CR Nanomaterials: A Membrane-based Synthetic Approach. Science 1994, 266, 1961–1966. [PubMed: 17836514]

(14). Shimizu T; Xie T; Nishikawa J; Shingubara S; Senz S; Gosele U Synthesis of Vertical High-Density Epitaxial Si(100) Nanowire Arrays on a Si(100) Substrate Using an Anodic Aluminum Oxide Template. Adv. Mater 2007, 19, 917–920.

(15). Song B; Wu C; Chang J Dual Drug Release from Electrospun Poly(lactic-co-glycolic acid)/Mesoporous Silica Nanoparticles Composite Mats with Distinct Release Profiles. Acta Biomater. 2012, 8, 1901–1907. [PubMed: 22326789]

(16). Oh S; Daraio C; Chen LH; Pisanic TR; Frnones RR; Jin S Significantly Accelerated Osteoblast Cell Growth on Aligned TiO_2 Nanotubes. J. Biomed. Mater. Res. Part A 2006, 78, 97–103.

(17). Faghihi S; Azari F; Zhilyaev AP; Szpunar JA; Vali H; Tabrizian M Cellular and Molecular Interactions between MC3T3-E1 Pre-osteoblasts and Nanostructured Titanium Produced by High Pressure Torsion. Biomaterials 2007, 28, 3887–3895. [PubMed: 17568665]

(18). Lozano D; Hernandez-Lopez JM; Esbrit P; Arenas MA; Gomez-Barrena E; de Damborenea J; Esteban J; Perez-Jorge C; Perez-Tanoira R; Conde A Influence of the Nanostructure of Fdoped TiO_2 Films on Osteoblast Growth and Function. J. Biomed. Mater. Res., Part A 2015, 103, 1985–1990.

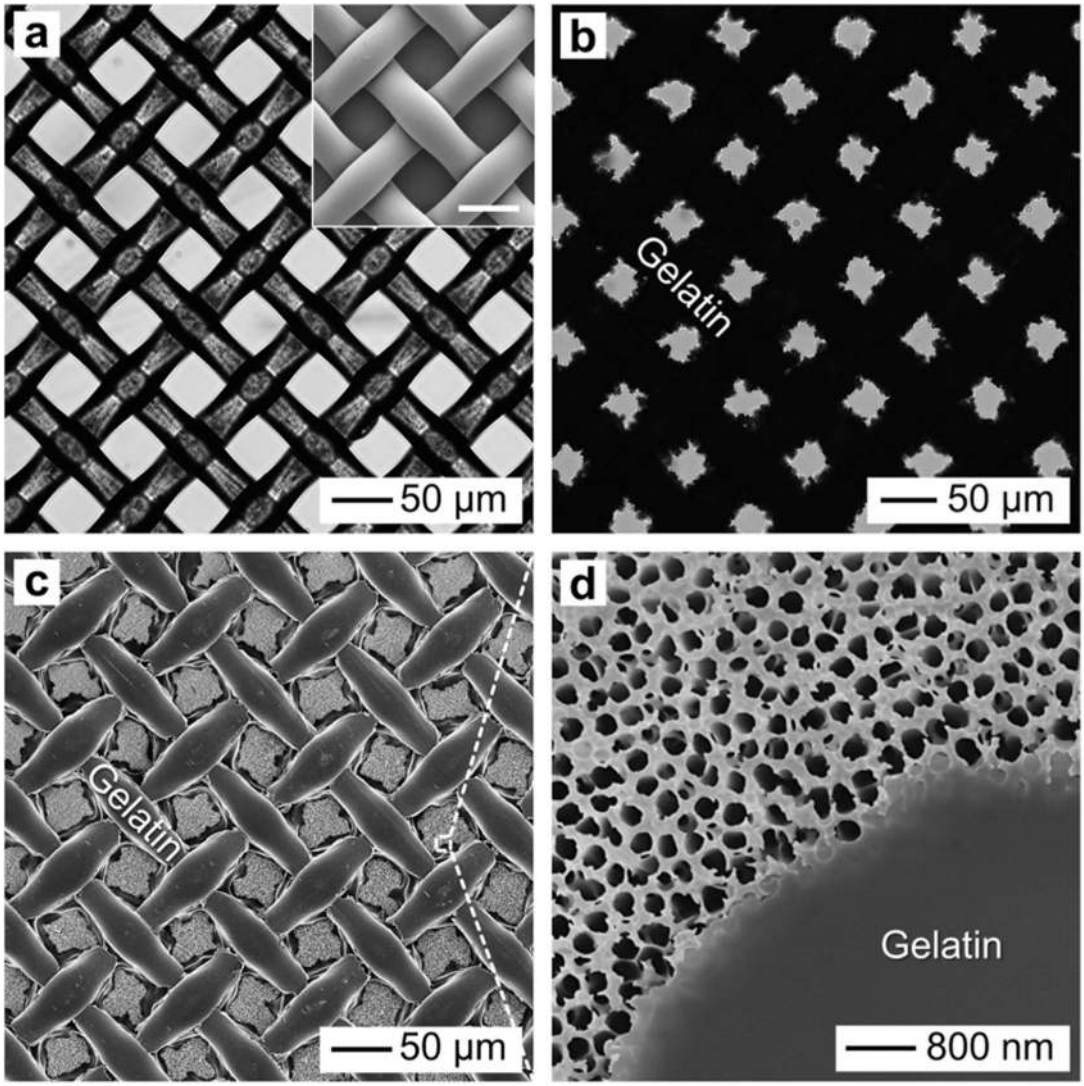

Figure 1.

Patterning the surface of an AAO membrane by transfer printing of gelatin with a nylon mesh. (a) Optical micrograph of a nylon mesh with a mesh opening of 41 μm and a spacing of 25 μm. The inset shows an SEM image of the mesh (scale bar: 50 μm), revealing the woven structure. (b) Optical micrograph of the nylon mesh after its surface had been coated with gelatin using electrospray. (c, d) SEM images of an AAO membrane, whose surface had been patterned with a meshed network of gelatin.

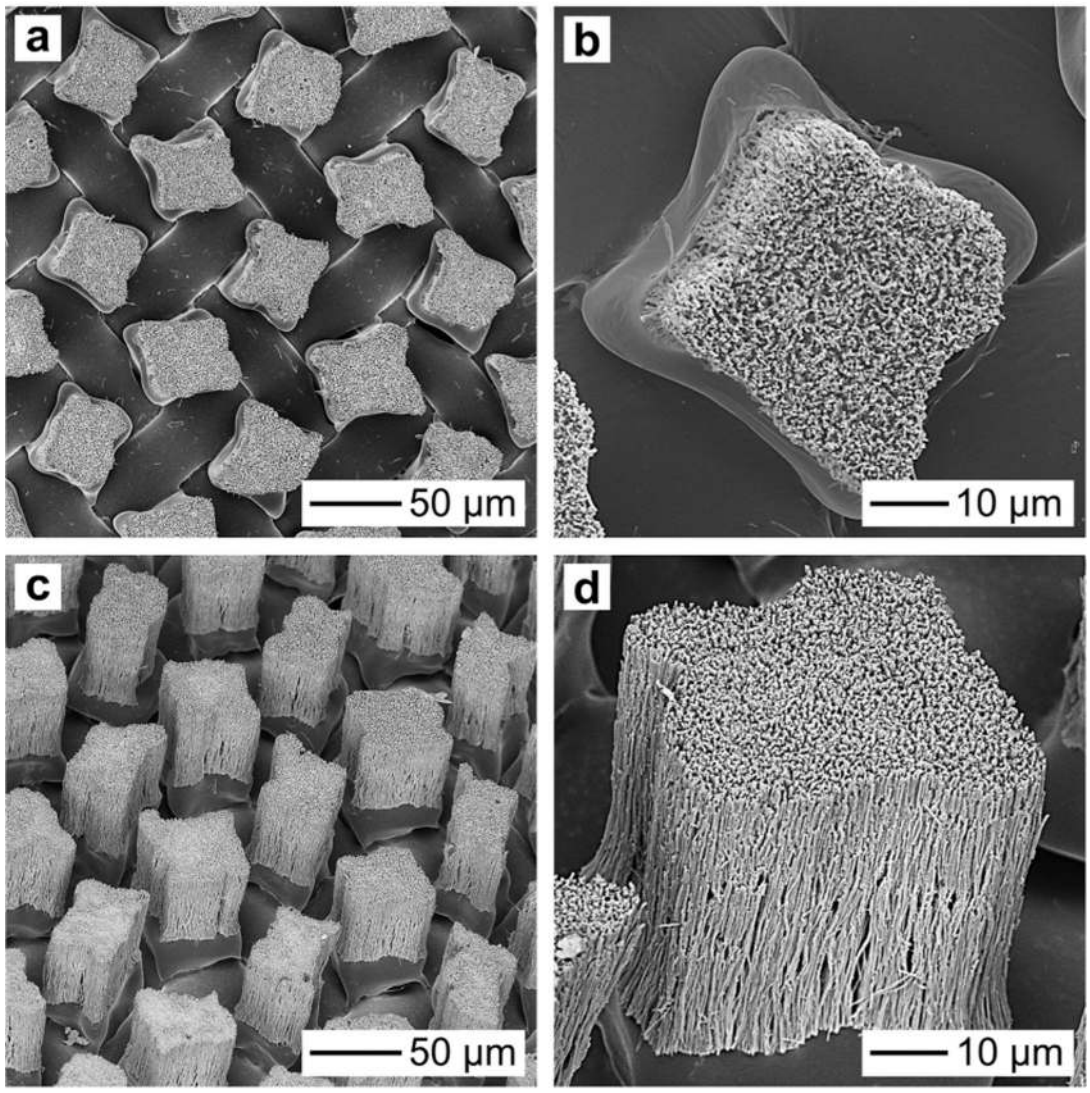

Figure 2.
SEM images of the micropatterend PLGA nanorod forests. (a, b) Top-view and (c, d) oblique-view images (tilting angle: 30°) at two different magnifications.

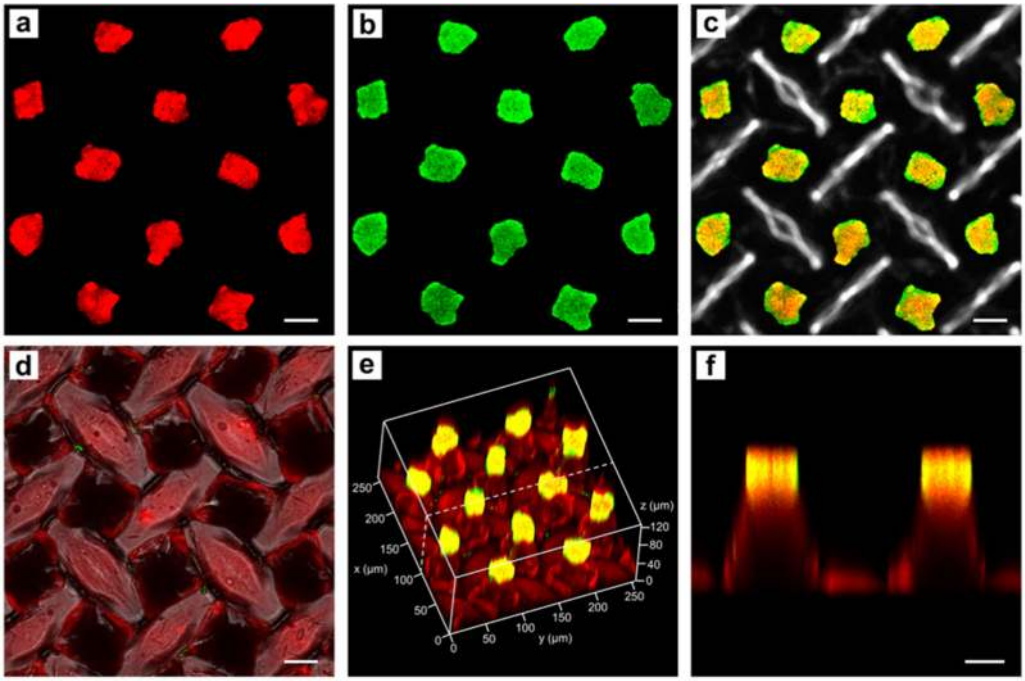

Figure 3.

Confocal images of the micropatterned nanorod forests loaded with dual model drugs. (a, b) Images recorded from the top focal plane showing the RhB encapsulated in the nanorods and the FITC-BSA physisorbed on the nanorods, respectively. (c) Overlay image at the top surface of the nanorod forests. (d) Overlay image at the base film. (e) 3D profile reconstructed from Z-stack images. (f) Cross-sectional image cut along the dash line indicated in e, showing the distribution of RhB and FITC-BSA relative to the nanorod forests along the Z-direction. Scale bar: 25 μm.

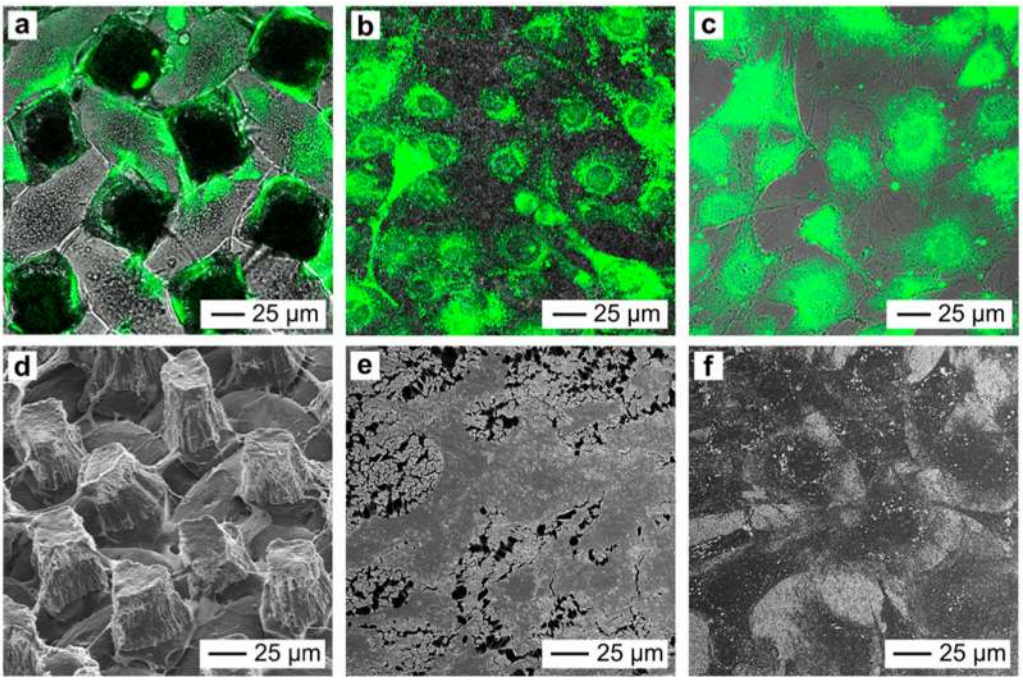

Figure 4.

MC3T3-E1 cells cultured on different substrates. (a–c) CLSM overlay images and (d–f) SEM images showing the adhesion and topological structures of MC3T3-E1 cells on (a, d) the micropatterned nanorod forests, (b, e) a nonpatterned nanorod forest, and (c, f) a glass coverslip. The cells were stained with calcein AM and fixed prior to imaging.

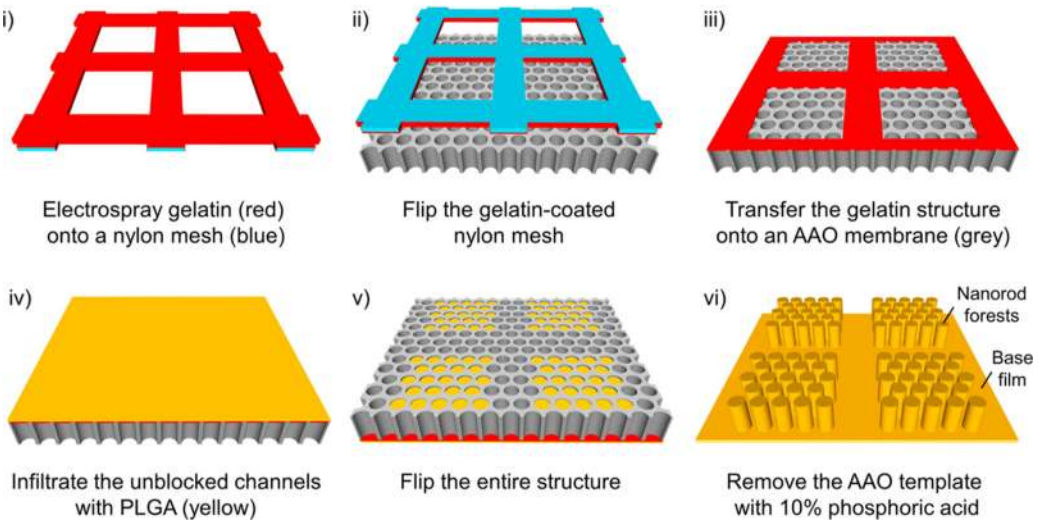

Scheme 1.

Schematic Illustration Showing the Fabrication of Micropatterned Nanorod Forests